ACS OMEGA

http://pubs.acs.org/journal/acsodf

Article

Extended Release of Metronidazole Drug Using Chitosan/Graphene Oxide Bionanocomposite Beads as the Drug Carrier

Gyanendra Kumar, Karan Chaudhary, Navin Kumar Mogha, Arun Kant, and Dhanraj T. Masram*

Cite This: *ACS Omega* 2021, 6, 20433−20444

Read Online

ACCESS | Metrics & More | Article Recommendations | Supporting Information

ABSTRACT: This study depicts the facile approach for the synthesis of chitosan/graphene oxide bionanocomposite (Chi/GO) beads via the gelation process. This is the first-ever study in which these Chi/GO beads have been utilized as a drug carrier for the oral drug delivery of metronidazole (MTD) drug, and investigations were made regarding the release pattern of the MTD drug using these Chi/GO beads as a drug carrier for a prolonged period of 84 h. The MTD is loaded on the surface as well as the cavity of the Chi/GO beads to result in MTD-Chi/GO bionanocomposite beads. The MTD drug loading was found to be 683 mg/g. Furthermore, the in vitro release patterns of pure drug and the drug encapsulated with Chi/GO beads are explored in simulated gastric as well as simulated intestinal fluids with phosphate-buffered saline (PBS) of pH 1.2 and 7.4, respectively. As-synthesized bionanocomposite beads have shown excellent stability and capacity for extended release of the MTD drug as compared to the pure drug in terms of bioavailability in both media. The cumulative release data are fitted with the *Korsmeyer-Peppas kinetics* and *first-order reaction kinetics* at pH 1.2 and 7.4. The synthesized bionanocomposite beads have good potential to minimize the multiple-dose frequency with the sustained drug release property and can reduce the side effects due to the drug.

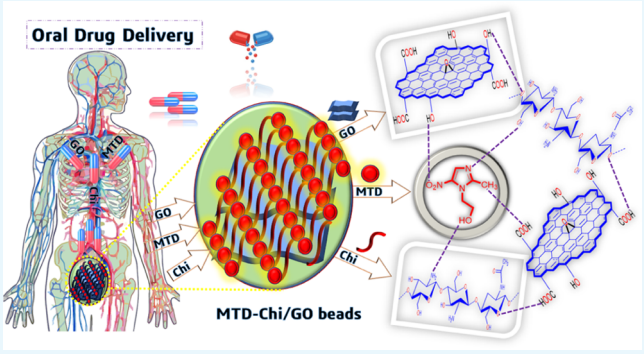

1. INTRODUCTION

Metronidazole (MTD) is an antibiotic drug that is used for the treatment of antibacterial and amoebic infections.[1] In amebiasis infections, the drug is used for oral dose depending on the age (18−64 years); e.g., for adults, the dose given is 500−750 mg thrice in a day. Moreover, smart bionanocomposites with extended drug-release properties will further improve the physiological and clinical properties in the treatment of amebiasis infections.[2,3] The literature has identified the possibility of in vitro release of drugs by the polymer nanocomposite.[4] Elzatahry et al. prepared chitosan nanoparticles as carriers for metronidazole and the result showed sustained release of drug for 12 h using these chitosan NPs.[5] Then, Sabbagh et al. used the chitosan-alginate polymeric nanocomposite for the incorporation of metronidazole and studied the release properties of metronidazole from the nanocomposite up to 63 h.[6] Further, in the available literature, extended-release formulation for the MTD drug is somewhat lacking due to the fast release of the drug from the available drug carriers. This issue can be addressed by cross-linking the therapeutics with some specially designed drug carriers. In general, up to 90% of the therapeutics are orally administered due to that route being noninvasive, less painful, and producing the maximum patient response. Moreover, oral drug delivery is effective in the case of anticancer drugs, protein drugs, and insulin, for the treatment of inflammation, Cohn's disease, and colon carcinoma.[7] Recently, researchers have been inclined toward the use of some organic polymers such as cellulose and starch and chemically modified organic polymers in various applications due to their various advantages such as biodegradability, large surface area, surface functional groups, good mechanical properties, hydrophilic nature, renewability, biocompatibility, and nontoxicity.[8−13] Further, polymer alginate has been used in drug delivery systems due to its excellent biocompatibility and low toxicity.[14]

Chitosan (Chi) is a natural polycationic biopolymer. It has good adsorbent properties for use in wastewater treatment and drug delivery applications.[15,16] Chi is composed of the β-(1-4)-linked 2-amino-2-deoxy-D-glucose unit, which is the deacetylation derivative of chitin. Chitosan is a multifunctional biopolymer due to the presence of abundant hydroxyl (−OH) and amino ($-NH_2$) groups, which allow chemical modifications.[17−19] Furthermore, chitosan has excellent properties such as lower toxicity, antibacterial activity,

Received: May 8, 2021
Accepted: July 20, 2021
Published: July 29, 2021

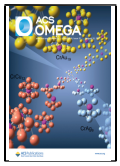

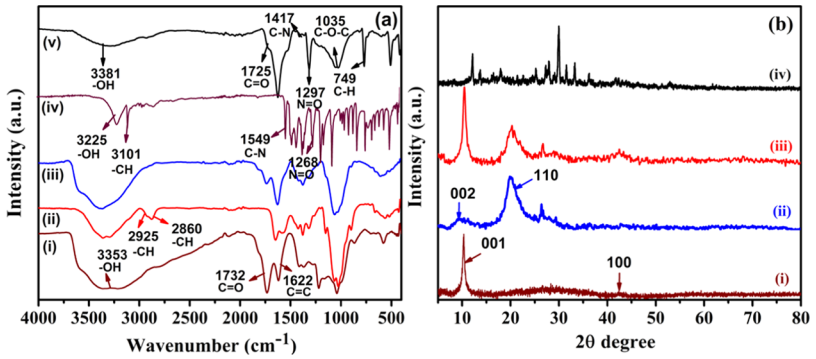

Figure 1. (a) FTIR spectra of (i) GO, (ii) chitosan, (iii) Chi/GO, (iv) pure MTD, and (vi) MTD-Chi/GO bionanocomposite beads, and (b) XRD of (i) GO, (ii) chitosan, (iii) Chi/GO, and (iv) MTD-Chi/GO bionanocomposite beads.

biocompatibility, biodegradability, and swelling properties for the drug delivery system.[20,21] Therefore, chitosan polymer is a more preferred option for drug delivery systems due to its well-known biopolymer, low cost, and use in medical treatment.[22−25] It has attracted attention in various biomedical and pharmaceutical processes such as drug/gene/vaccine delivery and manufacturing of cosmetic products due to its biodegradable nature that prevents polymer accumulation in the human body.[26−28] However, biodegradation affects drug activity, toxicity, and must be carefully controlled for oral drug delivery. Recently, chitosan has been cross-linked with various materials for higher stability.[29−33] Carbon-based materials such as carbon nanotube (CNT), graphene (GR), and GO have been used for cross-linking Chi.[34−36] GO as a drug carrier was discovered in 2008 by Dai et al.; polyethylene glycol/GO was used as a novel drug nanocarrier for loading of anticancer drugs through noncovalent bonding.[37] The noncovalent approach is commonly used for the modification of GO with chitosan, which can be used for drug delivery.[38,39] Among the carbon-based materials, GO has been extensively used in drug delivery applications because of its nontoxicity and biocompatibility.[40,41] The characteristic features of GO are its monolayer two-dimensional honeycomb crystal structures containing randomly distributed polar functional groups on the surface and edges along with large specific surface areas.[42−44] This helps to carry the drugs via surface adsorption through hydrogen bonding as well as electrostatic interactions.[45] GO and its derivatives have been used in biomedical applications.[46−48] GO has a great ability to support the cross-linked polymer due to its mechanical properties, and this makes the GO−protein composite suitable for drug delivery application.[49] The graphene-based polysaccharides are water-dispersible, nontoxic, biodegradable, biocompatible, and used for drug delivery applications.[50] Some recent studies show that chitosan-based nanocomposites with nano clays (alumina, montmorillonite (MMT)), graphene oxide (GO), zeolite, and bentonite possess remarkable properties like a porous network structure, excellent swelling or deswelling, large surface area, high sorption capacity, biocompatibility, and eco-friendliness.[51−53]

The aim of this work is to prepare a bionanocomposite material that can be used for efficient oral drug delivery of the MTD drug and has a prolonged drug release profile. Herein, we report the synthesis of economical MTD-Chi/GO bionanocomposite beads and their application in oral drug delivery. Metronidazole-chitosan/graphene oxide (MTD-Chi/GO) bionanocomposite beads were synthesized with variation in graphene oxide ratio (01−21mg) via the gelation process. These bionanocomposite beads have a high interconnected porosity, high mechanical strength, and a large surface area for sustained and controlled release of the MTD drug. This work shows the first-ever use of Chi/GO beads as a drug carrier agent for oral drug delivery of the MTD drug, and investigations were made regarding the release pattern of the MTD drug from these Chi/GO beads as a drug carrier for a prolonged period of 84 h.

2. RESULTS AND DISCUSSION

2.1. Fourier-Transform Infrared Spectroscopy and Powder X-ray Diffraction Studies. Fourier-transform infrared spectroscopy (FTIR) of GO, chitosan, Chi/GO, and MTD-Chi/GO bionanocomposite beads was done to assign the functional groups and the chemical interaction between them. The spectrum of pristine GO is shown in Figure 1a(i); the peaks obtained for −OH at 3353 cm^{-1}, C═O at 1732 cm^{-1}, C═C at 1622 cm^{-1}, C−OH at 1211 cm^{-1}, and C−O−C at 1035 cm^{-1} indicate the presence of hydroxyl, carbonyl, unoxidized graphite domains, carboxylic, and epoxy groups, respectively.[54] The pure chitosan has characteristic peaks for −OH at 3423 cm^{-1}, symmetric and asymmetric stretching of −CH at 2925 and 2860 cm^{-1}, respectively, and C═O stretching of amide I at 1651 cm^{-1}. The small band of the N−H bending of amide II was found at 1560 cm^{-1}, whereas the presence of the C−N stretching of amide III was found at 1381 cm^{-1}. Furthermore, CH_2 bending and CH_3 stretching were confirmed by the presence of peaks at 1407 and 1363 cm^{-1}, respectively. The absorption bands at 1074 and 1025 cm^{-1} correspond to the C−O stretching, which is shown in Figure 1a(ii).[55] The spectrum for the Chi/GO nanocomposite is shown in Figure 1a(iii) and contains all peaks similar to GO and chitosan; e.g., the peak of −OH is present at 3396 cm^{-1} and the peak for C═O stretching is present at 1739 cm^{-1}. Additionally, the peak for the C═O stretching of amide I is found to be at 1651 cm^{-1}, whereas peaks for C−N stretching and C−O stretching were obtained at 1381 and 1059 cm^{-1}, respectively.[56] The FTIR of a pure MTD drug is represented in Figure 1a(iv). The peaks were obtained at 3225, 3101, 1549, and 1268 cm^{-1}, which can be ascribed to the −OH, −CH, −CN, and −N═O functional groups of the pure MTD drug.

In the case of the MTD-Chi/GO bionanocomposite, the peak for −OH stretching was obtained at 3391 cm^{-1} with slightly reduced intensity. The peak obtained for the C═O stretching at 1725 cm^{-1} was small as compared to that of GO. The C−N stretching peak was found at 1417 cm^{-1} and the

https://doi.org/10.1021/acsomega.1c02422
ACS Omega 2021, 6, 20433−20444

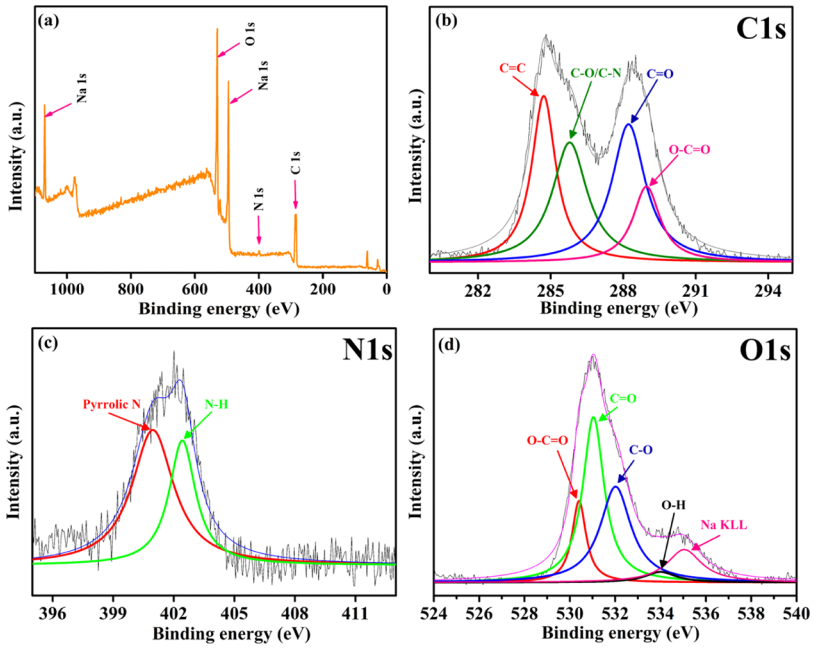

Figure 2. XPS (a) survey spectrum, (b) deconvoluted C 1s spectrum, (c) deconvoluted N 1s spectrum, and (d) deconvoluted O 1s spectrum of the MTD-Chi/GO bionanocomposite.

peak of N═O was present at 1297 cm^{-1}, which show the presence of the MTD drug in the bionanocomposite material. In conclusion, the peaks are slightly shifted due to the hydrogen bonding as well as electronic interactions of chitosan, graphene oxide, and the drug (Figure 1a(iv).[29]

Powder X-ray diffraction (P-XRD) patterns of the GO, chitosan, Chi/GO, and MTD-Chi/GO bionanocomposite beads are recorded between 5 and 80° of the 2θ diffraction angle. The P-XRD pattern of pristine GO is shown in Figure 1b(i), which contains two characteristic peaks at 2θ = 10.42 and 42.36° corresponding to the ⟨001⟩ and ⟨100⟩ planes, respectively, showing that the graphite is fully oxidized into graphene oxide.[57,58] In the P-XRD pattern for pure chitosan (Figure 1b(ii)), there are two characteristic peaks at 2θ = 9.51 and 19.99° corresponding to crystallographic planes ⟨002⟩ and ⟨110⟩, respectively.[59] The P-XRD pattern of the Chi/GO nanocomposite shows four noticeable peaks at 2θ = 10.42, 20.30, 26.69, and 42.36°; these peaks indicate the chitosan cross-linking with GO (Figure 1b(iii)). As per the literature, the P-XRD pattern of the pure drug has several peaks at 2θ = 12.11, 13.73, 16.17, 17.06, 17.95, 19.37, 20.99, 23.10, 24.59, 25.21, 27.31, 29.28, 29.68, 31.19, and 33.22°.[60] Furthermore, the P-XRD pattern of the MTD-Chi/GO bionanocomposite beads contains peaks at 2θ = 12.09, 13.61, 17.87, 25.17, 27.29, 27.91, 30.05, 31.55, 33.23, 36.27, and 42.36° as shown in Figure 1b(iv), which reveal the formation of the desired MTD-Chi/GO bionanocomposite beads.

2.2. X-Ray Photoelectron Spectroscopy (XPS) Studies. XPS study of the MTD-Chi/GO bionanocomposite beads was performed to understand the chemical composition of the nanocomposite. Figure 2a depicts the complete survey XPS spectrum of the MTD-Chi/GO bionanocomposite, which confirms that C, N, O, and Na are the main elements present in the nanocomposite. The C 1s deconvoluted XPS spectrum of the MTD-Chi/GO bionanocomposite (Figure 2b) contains four peaks centered at 284.7, 285.8, 288.2, and 288.9 eV, which are assigned to C═C, C−O/C−N, C═O, and O−C═O functionalities, respectively.[61,62] Also, Figure 2c shows the deconvoluted XPS spectrum for the N 1s level and it contains two peaks centered at 400.9 and 402.4 eV that are assigned to pyrrolic-N and N from the ammonia group, respectively.[63,64] Further, the deconvoluted spectrum of the O 1s level is shown in Figure 2d, which contains five peaks centered at 530.4, 531.0, 532.0, 533.9, and 535.0 eV that have been ascribed to O−C═O, C═O, C−O, O−H, and the sodium Auger peak, respectively.[62,65] Overall, the presence of peaks for different groups such as C═C, C−O, C−N, C═O, O−C═O, O−H, pyrrolic-N, and N from the ammonia group reveals the formation of the desired MTD-Chi/GO bionanocomposite beads.

2.3. Thermogravimetric Analysis (TGA). TGA is employed to investigate the thermal stability and decomposition of the composite materials. The TGA curves of Chi, Chi/GO, and the MTD-Chi/GO bionanocomposite were characterized in-between 25 and 600 °C, which is depicted in Figure S1. The TGA of pure chitosan shows three weight losses: the first weight loss that occurs between 25 and 150 °C can correspond to the loss of water molecules. The second and the major weight loss is found in between 150 and 300 °C (~270 °C), which corresponds to the removal of the functional groups (−OH, C−O, N−H) present on the chitosan molecule. The third weight loss occurred between 300 and 600 °C, which is due to the full collapse and is illustrated in Figure. S1i. The curve of the Chi/GO nanocomposite shows three weight losses: the first decomposition of Chi/GO is found between 25 and 150 °C and can be attributed to the loss of water molecules.[66] The second decomposition occurred in between 150 and 300 °C, which can correspond to the loss of functional groups (−OH, C═O, C−O, C−O−C, N−H) on the Chi/GO nanocomposite. The third weight loss occurred between 300 and 600 °C, which is due to the full collapse and is shown in Figure S1ii. The curve of MTD-Chi/GO bionanocomposite beads shows three weight losses: the first weight loss of the MTD-Chi/GO bionano-

https://doi.org/10.1021/acsomega.1c02422
ACS Omega 2021, 6, 20433−20444

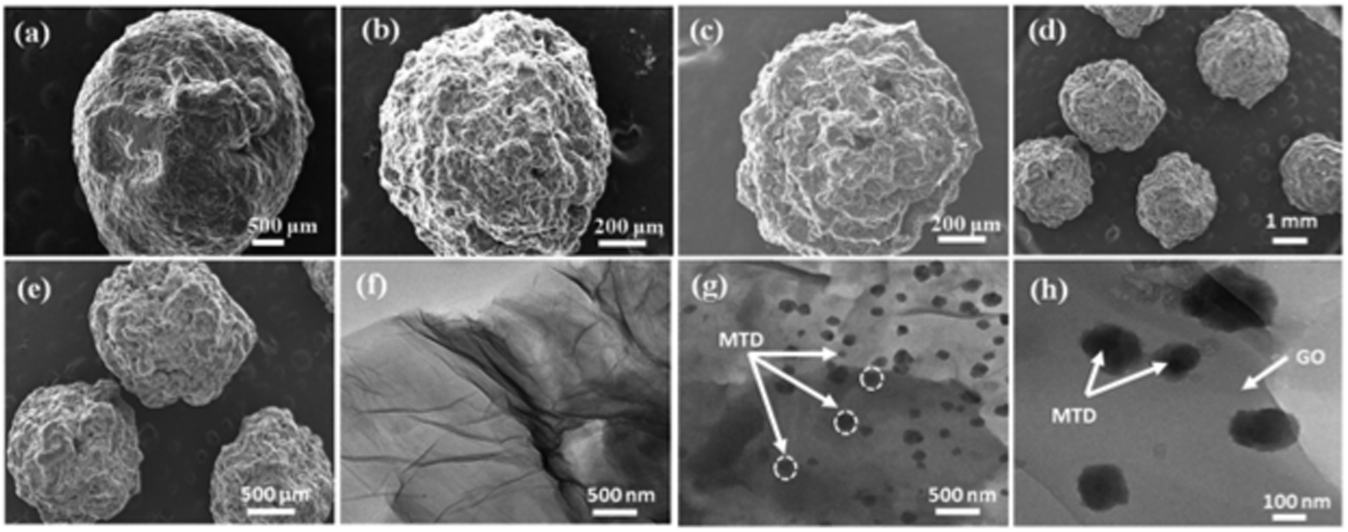

Figure 3. SEM images showing the surface morphologies for (a) dry beads of pure chitosan, (b) dry beads of MTD-Chi, and (c–e) dry beads of MTD-Chi/GO bionanocomposite. TEM images of (f) pristine GO and (g, h) MTD-Chi/GO bionanocomposite beads.

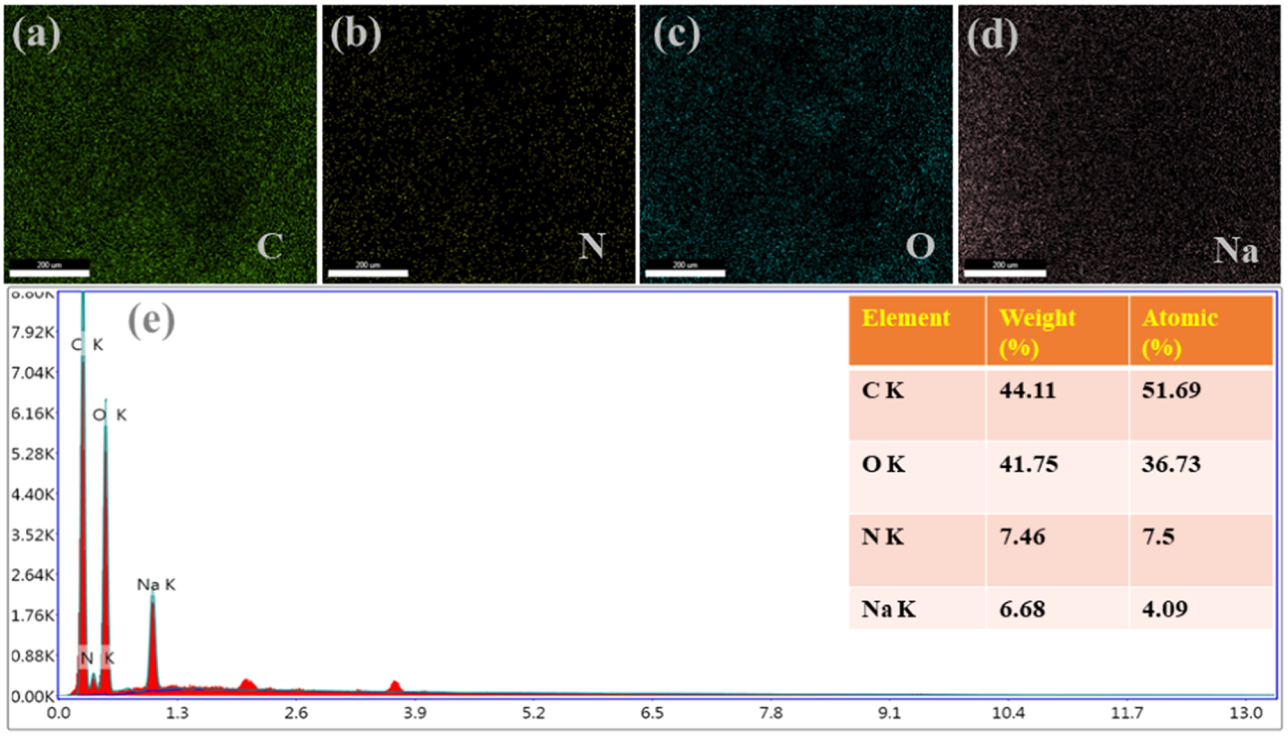

Element	Weight (%)	Atomic (%)
C K	44.11	51.69
O K	41.75	36.73
N K	7.46	7.5
Na K	6.68	4.09

Figure 4. EDS mapping, including (a) C, (b) N, (c) O, (d) Na, and (e) elements of the MTD-Chi/GO bionanocomposite beads.

composite beads is between 25 and 150 °C, which is due to the removal of the water molecules. The second weight loss can correspond to the loss of functional groups (−OH, C═O, C−O, C−O−C, N−H) present in MTD-Chi/GO between 150 and 300 °C.[67] The third weight loss, between 300 and 600 °C, is due to the full collapse of the MTD-Chi/GO bionanocomposite beads, as shown in Figure S1iii. Further, the main weight loss in the case of Chi occurred at ∼270 °C, which was attributed to the Chi group removal, but in the case of Chi/GO and the MTD-Chi/GO bionanocomposite, there was a difference in the thermal stability, and the main weight loss was observed at ∼210 °C due to removal of the oxygen-containing groups of GO present in the composites. As for pure GO, the thermal stability is low, and at around 100 °C the oxygen-containing groups are lost, whereas GO with Chi in these composites improved the thermal stability of GO due to the cross-linking of Chi and GO and weight loss occurred approximately at 210 °C.[68]

2.4. Morphological Characterization. The surface morphologies of pure chitosan, MTD-Chi, MTD-Chi/GO bionanocomposite beads, and GO were studied by scanning electron microscopy (SEM) techniques and are illustrated in Figure 3. The SEM micrographs for dry beads of pure chitosan (Figure 3a) clearly depict a spherical shape and the surface appears more smooth and regular. Figure 3b shows the SEM micrograph for MTD-Chi, which reveals the special shape of the material, but the surface of the MTD-Chi bead is rough and irregular on the addition of the MTD drug. Figure 3c–e

https://doi.org/10.1021/acsomega.1c02422
ACS Omega 2021, 6, 20433−20444

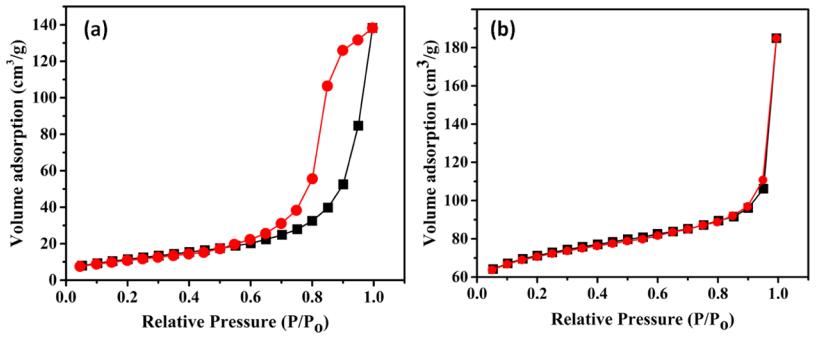

Figure 5. N_2 adsorption−desorption isotherm of (a) Chi/GO and (b) MTD-Chi/GO bionanocomposite beads.

shows the TEM micrograph of the MTD-Chi/GO bionanocomposite beads at different magnifications. From Figure 3c, it is clear that the bead has a spherical shape, but the inclusion of GO as well as the MTD drug makes the surface more rough and irregular. Further, Figure 3d−f shows several beads having spherical morphology, and it was calculated that the diameter of the beads varies in the range of 1.50−1.85 mm, which shows that they are of the same sizes. Also, the average diameter of beads was calculated to be ∼1.67mm (using ImageJ software).

Further, transmission electron microscopy (TEM) was performed, and the micrographs for GO and MTD-Chi/GO bionanocomposite beads are shown in Figure 3f−h. TEM micrographs of GO (Figure 3f) reveal the characteristic wrinkled sheet structure of pristine GO. Further, the TEM micrograph for the MTD-Chi/GO bionanocomposite shown in Figure 3g,h reveals that the addition of Chi resulted in the covering of the surface of GO and its characteristic feature is not visible. Further, it can be observed that there is the stacking of sheets. Moreover, TEM was performed for dried MTD-Chi/GO bionanocomposite beads. Figure 3g,h depicts the deposition of particles on the surface and in-between the Chi/GO, which can be attributed to the MTD particles (around 20−100 nm) formed due to the accumulation of drug molecules during the drying of beads.

The energy-dispersive X-ray (EDS) analysis was employed for further investigation of MTD-Chi/GO bionanocomposite beads and the results obtained are shown in Figure 4. The EDS spectrum tells the purity and complete chemical composition of the nanocomposites. The obtained elemental maps for the elements of the MTD-Chi/GO bionanocomposite beads are shown in Figure 4a−d. The EDS spectra of MTD-Chi/GO are shown in Figure 4e, revealing that carbon, oxygen, and nitrogen are the elements that are present. Also, the EDS results show the presence of sodium that is left even after washing.

2.5. Surface Area and Pore-Size Analysis. BET analysis was performed to study the porous structure of Chi/GO and MTD-Chi/GO composites, and the obtained N_2 adsorption−desorption isotherm is shown in Figure 5. The isotherms for both Chi/GO and MTD-Chi/GO composites show a Type III isotherm with a H3 hysteresis loop. Further, the data obtained from BET analysis about the surface area, pore volume, and pore diameter for both composites have been tabulated in Table 1. Moreover, Chi/GO and MTD-Chi/GO composites are microporous materials as their average pore diameter is 200 and 52 Å (20 and 5.2 nm), respectively. It is observed that when MTD was incorporated in the MTD-Chi/GO composite, the average pore diameter decreased in comparison to that of the Chi/GO composite, which depicts the encapsulation of the MTD drug in the porous structure of the composite.

Table 1. Textural Features of Chi/GO and MTD-Chi/GO Bionanocomposite Beads

samples	S_{BET} $(m^2 \cdot g^{-1})^a$	$V_{(total)}$ $(cm^3 \cdot g^{-1})^b$	d (Å)^c
Chi/GO	42	0.21	200
MTD-Chi/GO	217	0.28	52

^{a}Multipoint BET surface area. ^{b}Total pore volume at $P/P_o(N_2)$. ^{c}Average pore diameter.

2.6. Digital Photograph Visualization of MTD-Chi/GO Bionanocomposite Beads. The morphologies of pure chitosan, MTD-Chi, and MTD-Chi/GO bionanocomposite beads were investigated using digital photographs, as shown in Figure 6. The photographs for the wet and dry beads of pure chitosan are shown in Figure 6a,e. Further, photographs for the wet and dry beads of the MTD-Chi nanocomposite are shown in Figure 6b,f. Moreover, photographs for the wet and dry beads of the MTD-Chi/GO bionanocomposite are presented in Figure 6c,g. It can be observed from the images that the wet and dry beads of MTD-Chi/GO bionanocomposite are spherical, which was also observed from SEM. The diameter for the wet bead was measured to be about 3−4 mm (Figure 6d), whereas the diameter for the dry bead was measured to be about 0.5−1 mm (Figure 6h) using a scale. As we know that GO has plenty of oxygen-containing functional groups that afford strong interactions with water, the swelling property of GO increases in an aqueous solution.[69,70] When weighed, it was found that the weight of five dry beads of the MTD-Chi/GO bionanocomposite bead was 14.91 mg, whereas the weight of five wet beads was obtained to be 43.53 mg. This reveals the excellent swelling property of the as-synthesized nanocomposite beads.

2.6.1. Encapsulation Efficiency of MTD in the Beads. The encapsulation efficiency was calculated by UV−visible spectrophotometry. The encapsulation efficiency (EE) is generally expressed in percentage as defined in eq 1.

$$\mathrm{EE} = \frac{\text{amount of MTD retained by Chi/GO bionanocomposite beads}}{\text{initial amount of MTD used}} \quad (1)$$

The percentages of MTD encapsulated in the Chi/GO nanocomposite beads are listed in Table 2. For MC1 to MC8, GO is not used, and only chitosan (50 mg) and the MTD drug are used for bead preparation. A high encapsulation efficiency is found at 26.302 and 35.100 at drug amounts of 30 and 40 mg, respectively. After that, the amount of MTD was fixed to carry out further experiments. Now, the amount of MTD drug

https://doi.org/10.1021/acsomega.1c02422
ACS Omega 2021, 6, 20433−20444

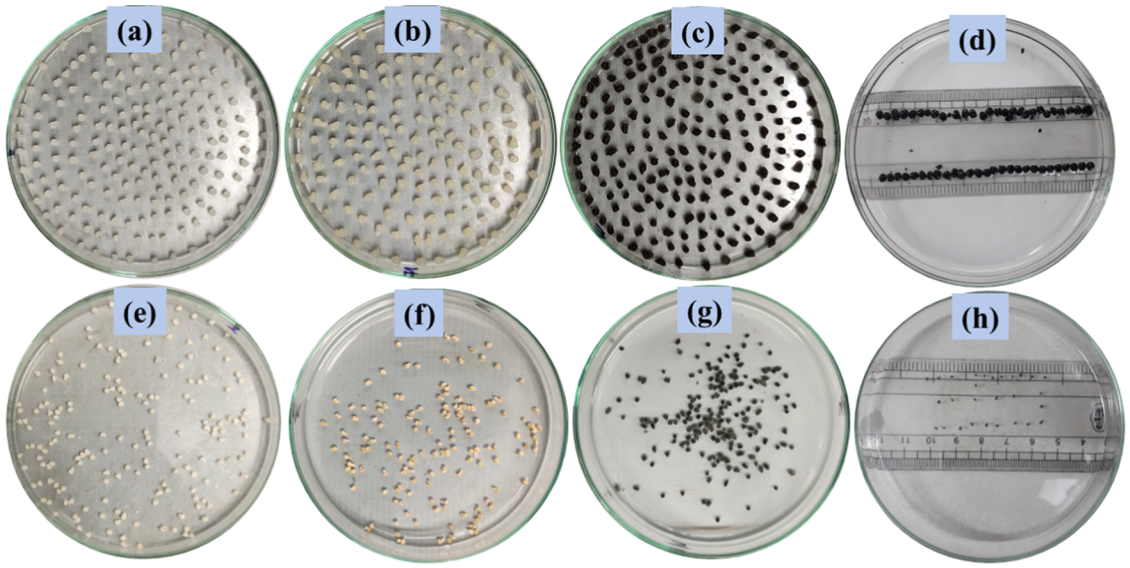

Figure 6. Digital photograph showing bionanocomposite beads of the (a and e) pure wet and dry chitosan beads, (b and f) MTD-Chi wet and dry beads, (c and g) MTD-Chi/GO bionanocomposite wet and dry beads, and (d and h) MTD-Chi/GO bionanocomposite wet and dry beads with scale measurements.

Table 2. MTD Encapsulated in Chi/GO Bionanocomposite Beads[a]

code of beads	chitosan (mg)	GO (mg)	MTD (mg)	EE of MTD (%)
MC1	50		05	04.127
MC2	50		10	09.695
MC3	50		15	09.779
MC4	50		20	16.385
MC5	50		25	20.190
MC6	50		30	26.302
MC7	50		40	34.975
MC8	50		40	35.100
MCG9	50	01	40	35.417
MCG10	50	02	40	36.063
MCG11	50	03	40	36.432
MCG12	50	04	40	36.912
MCG13	50	05	40	36.406
MCG14	50	08	40	34.362
MCG15	50	10	40	33.254
MCG16	50	15	40	36.129
MCG17	50	18	40	36.124
MCG18	50	21	40	36.120

[a]EE = encapsulation efficiency.

used is 40 mg, that of chitosan is 50 mg, and the amount of GO was varied (01−21 mg). The maximum encapsulation efficiency was found to be 36.129% when 4 mg of graphene oxide was used. Further, on increasing the amount of GO the encapsulation efficiency slightly decreased. Finally, based on the results obtained, nanocomposite materials with maximum encapsulation efficiency (coded as MC6, MC8, MCG12, and MCG16) were used in drug release studies.

2.6.2. Quantitative Estimation of MTD in 0.5M Sodium Hydroxide Solution. A stock solution of MTD drug (100 ppm) was prepared in a 0.5 M NaOH solution. Additionally, a series of known solutions (1−20 ppm) were prepared in a 25 mL volumetric flask. The absorbance of each solution was measured at 320 nm (Figure 7a). From the calibration plot between the concentration (ppm) and absorbance (Figure 7b) for the prepared series of solutions, the slope and intercept were calculated and were found to be 0.0444 and 0.1710, respectively. The correlation coefficient (R^2) is found to be 0.9972 as shown in Figure 7b.

2.7. *In Vitro* Drug Release Profile. *In vitro* drug release is performed to evaluate the release capability of the drug from the MTD-Chi/GO bionanocomposite beads in the simulated gastrointestinal tract (GIT) conditions. For the release process of the drug from the bionanocomposite beads, it is kept in a

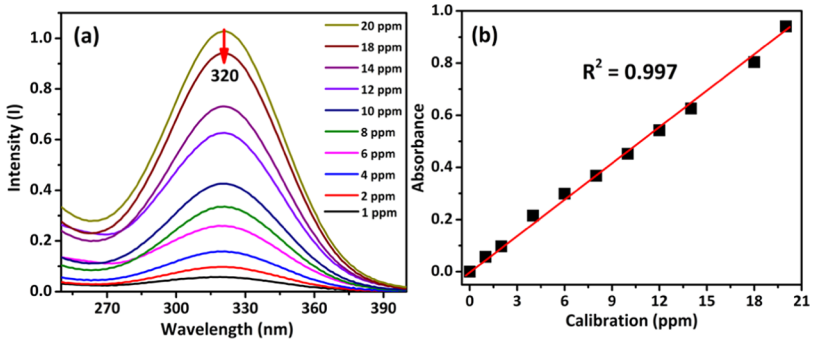

Figure 7. (a) Absorbance curve and (b) calibration curve of MTD in 0.5M NaOH solution.

https://doi.org/10.1021/acsomega.1c02422
ACS Omega 2021, 6, 20433−20444

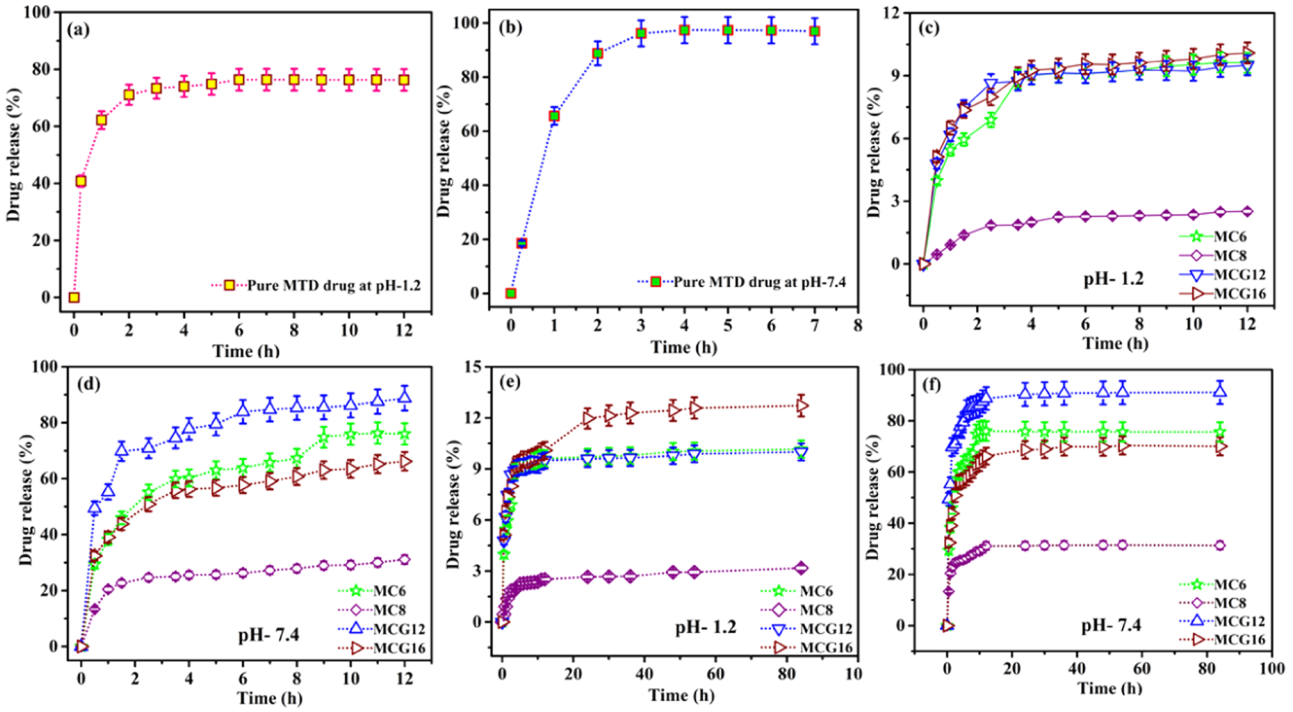

Figure 8. Drug release of pure MTD at (a) pH 1.2 and (b) pH 7.4. (c) Drug release from MC6, MC8, MCG12, and MCG16 at pH 1.2 for 12 h (d) and at pH 7.4 for 12 h. Drug release from MC6, MC8, MCG12, and MCG16 at (e) pH 1.2 for 84 h and (f) pH 7.4 for 84h.

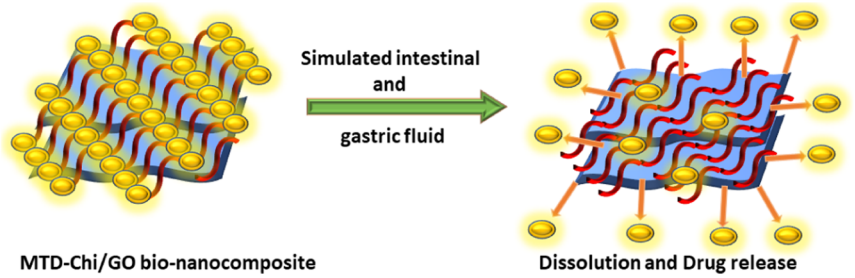

Figure 9. Schematic drug release diagram of the MTD-Chi/GO bionanocomposite.

dialysis bag (release of drug using a dialysis membrane and a high-retention seamless cellulose tubing of flat width 32 mm (1.3 in.), Sigma-Aldrich, *in vitro* release (outer volume = 500 mL, paddle rpm = 100)) and immersed into 500 mL of HPLC grade water at 37 °C. The release process was performed in acidic and basic conditions using phosphate-buffered saline (PBS) in simulated gastric fluid (PBS, pH 1.2) and simulated intestinal fluid (PBS, pH 7.4) separately over an extended period of 84 h with continuous stirring at 100 rpm in 8 bowls using a dissolution test apparatus. At regular intervals, a 5 mL solution was collected, while a 5 mL fresh PBS solution was added to maintain the volume of the release system. The MTD drug release at pH 1.2 and 7.4 is determined at 320 nm using UV−visible spectroscopy. The release pattern was studied for four selected compositions (MC6, MC8, MCG12, and MCG16) and compared with that of pure MTD in simulated gastric and intestinal fluid. The pure MTD drug shows bust release; the drug release in the initial 2h was found to be 71.07 and 88.78% in the simulated gastric fluid (pH 1.2) and intestinal fluid (pH 7.4), respectively. The drug release percentage is higher at pH 7.4 as compared to pH 1.2. But, these obtained results are not desirable as they will lead to multiple doses of the drug; the results are shown in Figure 8a,b. In the case of the bionanocomposite beads, the release of the drug for MC6, MC8, MCG12, and MCG16 was found to be 6.89, 1.85, 8.65, and 7.99%, respectively, at pH 1.2 in the initial 2h. Further, the release profile of the drug for MC6, MC8, MCG12, and MCG16 in the simulated gastric fluid up to 12 h is given in Figure 8c,d.

After 8 h, drug release was 9.26, 2.31, 9.27, and 9.62% at pH 1.2 for MC6, MC8, MCG12, and MCG16, respectively. Afterward, 12 h drug release was found to be 9.61, 2.51, 9.50, and 10.09% at pH 1.2 for MC6, MC8, MCG12, and MCG16, respectively. These values show a sustained release of the drug, which will make it more bioavailable as compared to pure MTD in simulated gastric fluid.

In the simulated intestinal fluid (pH 7.4), the pure MTD drug showed a fast release. 97.39% of the drug was released within 4 h and after that, it remained constant up to 12 h, which is not the desirable release for a pure drug. The drug release profile for MC6, MC8, MCG12, and MCG16 is shown in Figure 8e,f. The MC6 release of the drug is found to be 67.27 and 75.88% at pH 7.4 after 8 and 24 h, respectively. After that, the release remains constant up to 84 h. Further, the drug release from MC8 at pH 7.4 is found to be 27.89 and 31.19% at 8 and 24 h, respectively, and after that, it remains

https://doi.org/10.1021/acsomega.1c02422
ACS Omega 2021, 6, 20433−20444

Table 3. Kinetics Release of the Calculated Data of Different Nanocomposite Beads in PBS Solution at pH 1.2 and 7.4

	PBS, pH 1.2				PBS, pH 7.4			
	Korsmeyer-Peppas		*First order*		*Korsmeyer-Peppas*		*First-order*	
code	R^2	K_{kp}, h^{-n}	R^2	k_1, h^{-1}	R^2	K_{kp}, h^{-n}	R^2	k_1, h^{-1}
MC6	0.8959	0.2629	0.6662	0.0042	0.9497	0.2799	0.9182	0.0871
MC8	0.8426	0.4503	0.7000	0.0014	0.8572	0.2016	0.7723	0.0134
MCG12	0.8064	0.1813	0.5424	0.0028	0.9342	0.1751	0.8960	0.1152
MCG16	0.9127	0.1918	0.6947	0.0035	0.9503	0.2086	0.8659	0.0504

constant up to 84 h. MCG12 drug release was found to be 85.29 and 90.34% at pH 7.4 at 8 and 24 h, respectively, and a maximum of 90.91% was reached up to 48 h; after this, it remains constant up to 84 h. MCG16 drug release was found to be 60.75 and 68.70% at 8 and 24 h, respectively, and after this, it remains constant up to 84 h. In conclusion, the synthesized MTD-Chi/GO bionanocomposite beads MC6, MC8, MCG12, and MCG16 showed better drug release patterns over an extended period as compared to pure MTD drug in both media. Therefore, the MTD-Chi/GO bionanocomposite beads are useful for future applications due to their minimizing the multiple-dose frequency with the possibility of better patient compliance.

2.8. Drug Release Kinetics. Taking into account all of the abovementioned, various factors can affect the dissolution of the MTD drug, such as the stirring speed, temperature, and composition of the dissolution media. Drug release models have a major application, and the best-describing phenomena of the physicochemical properties as well as composites of the MTD drug to Chi/GO ratio that govern the release from the formulation are represented in Figure 9.

To better understand the release mechanism of the MTD drug from the Chi/GO nanocomposite beads in the form of a cumulative release, the data is fitted with the *Korsmeyer-Peppas formula* using eq 2.

$$\frac{M_t}{M_\infty} = Kt^n \tag{2}$$

where M_t is the amount of drug released at time t, M_∞ is the amount of drug released as the time approaches infinity, K is the rate constant, and n is the diffusional exponent characteristic of the drug release mechanism.[71] The fitting coefficients (R^2) are calculated and represented in Table 3 at pH 1.2 and 7.4 for the PBS solution. The fitting data can be compared with the real relationship between the response data parameters.

In the *first-order kinetics model*, a constant fraction of drug in the body is eliminated per unit of time.[72] The *first-order model* indicates that the release rates are directly proportional to the concentration of the drug formula using eq 3.

$$\log C_t = \log C_0 - \frac{K_1 t}{2.303} \tag{3}$$

where C_t is the amount of drug released at time t, C_0 is the initial amount of the drug (most of the time $C_0 = 0$), and K_1 is the first order of the drug release constant. The drug release fitted data is given in Table 3 for the PBS solution at pH 1.2 and 7.4 respectively. The kinetic profile for MC6, MC8, MCG12, and MCG16 according to *Korsmeyer-Peppas* and the *first-order kinetics* are shown in Figure S3a–h at pH 1.2 and 7.4, respectively. In conclusion, MCG16 best fitted *Korsmeyer-Peppas* due to its correlation coefficient, which was found to be R^2 = 0.9127 in PBS at pH 1.2. In the case of MC6, it fitted both *first-order model* as well as *Korsmeyer-Peppas* in PBS at pH 7.4. Furthermore, MCG8 and MCG16 well fitted *Korsmeyer-Peppas* in PBS at pH 7.4. The drug release kinetic models of multiple release procedures are implemented as a helpful tool to better explain the drug delivery systems and release mechanisms of the fundamental theory. Moreover, Ritger and Peppas and Korsmeyer and Peppas have developed an empirical equation to analyze both Fickian and non-Fickian release of a drug from a swelling and a nonswelling polymeric delivery system. Moreover, this model fits in values such as $0.45 < n < 0.89$ for non-Fickian release (anomalous) from cylinders (nonswellable matrix) and $0.43 < n < 0.85$ for non-Fickian release (anomalous) from nonswellable spherical beads,[73] which is shown in Table 4. To find out the exponent n, the portion of the release curve $\frac{M_t}{M_\infty} < 0.6$ should only be used. In conclusion, codes MC6, MC8, MC12, and MC16 show nonswellable matrix diffusion because the drug release exponent n is equal to or less than 0.5.

Table 4. Calculated *Korsmeyer-Peppas* (Values of n) of Different Nanocomposite Beads at pH 1.2 and 7.4

release exponent (n)	drug transport mechanism	drug release mechanism
$n < 0.5$	Quasi-Fickian diffusion	nonswellable matrix diffusion
0.5	Fickian diffusion	
$0.5 < n < 1.0$	Anomalous (non-Fickian transport)	For both diffusion and relaxation (erosion)
1.0	Case II transport	Zero-order release
higher than 1.0	Super case II transport	(relaxation/erosion)

	Korsmeyer-Peppas (calculated value of n)	
code	**pH 1.2**	**pH 7.4**
M6	0.2701	0.287
M8	0.4643	0.207
M12	0.1877	0.1786
M16	0.1964	0.2159

2.9. Comparison Study. In previous studies, it has been found that GO and chitosan-based bionanocomposites have been used as drug delivery agents for different drugs and have shown sustainable drug release. The different studies based on GO and chitosan-based bionanocomposites as drug carriers have been compared with the present study in Table 5. From the table, it can be observed that the GO and chitosan-based bionanocomposites have been used for delivery of drugs such as ibuprofen (IBU), which had a release time of 100 h,[74] camptothecin (CPT), which had a release time of 72 h,[75] paclitaxel (PTX), which had a release time of 72 h,[47] sumatriptan succinate (SS), which had a release time of 50 h,[76] and famotidine (FMT), which had a release time of 12 h.[77] This shows that these GO and chitosan-based bionanocomposites have the potential for extended drug

https://doi.org/10.1021/acsomega.1c02422
ACS Omega 2021, 6, 20433−20444

Table 5. Drug Carrier Materials Compared with the Previous Studies on a Different Drug

carrier material	drug	release time (h)	refs
GO/CS	IBU	100	74
GO-CS	CPT	72	75
GO-CSN	PTX	72	47
CS/TPP/GO	SS	50	76
GO-CH	FMT	12	77
CHI/GO	MTD	84	present work

release. Here, it is the first-ever use of this bionanocomposite for loading and release study of the MTD drug, and we found that this material is efficient as a drug delivery agent for this drug.

3. CONCLUSIONS

We have successfully synthesized MTD-Chi/GO bionanocomposite beads and used them as an extended drug delivery system. The release profile of bionanocomposite beads (MC6, MC8, MCG12, and MCG16) was found for an extended period (up to 84 h) as compared to the pure MTD drug in simulated gastric (pH 1.2) and simulated intestinal fluid (pH 7.4). Consequently, the drug release data from *Korsmeyer-Peppas* and the *first-order reaction* in both media indicates the potential of the bionanocomposite to minimize multiple-dose frequencies with the possibility of better patient compliance. MTD-Chi/GO bionanocomposite beads enhanced the initial burst release content of the drug and increased the stability of the drugs against the harsh conditions of the gastrointestinal tract and simulated intestinal fluid. Thus, it also provided sustained, extended, and controlled release of the drug. The morphology of MTD-Chi/GO bionanocomposite beads is confirmed by SEM and TEM analysis; the dimensions are found to be 50−100 nm. Moreover, the EDS analysis of MTD-Chi/GO bionanocomposite beads is evidence for the composition of elements such as carbon, oxygen, nitrogen, and sodium, which is confirmed by the XPS techniques.

4. EXPERIMENTAL SECTION

4.1. Synthesis of Graphene Oxide (GO). GO was synthesized using a previously reported method with some minor modifications.[78,79] Briefly, 3.0 g of natural graphite powder was added to 400 mL of a mixture of (18:2) H_2SO_4/H_3PO_4, followed by the addition of $KMnO_4$ (9.0 g) in small lots of ∼250 mg per min with continuous stirring at 50 °C for 12 h. The reaction was cooled at room temperature and transferred to a container having crushed ice, followed by dropwise addition of 30% H_2O_2 (5.0 mL) solution. The color change from dark brown to bright yellow indicates the formation of GO. Afterward, the GO suspension is washed by centrifugation for 5 min at 5500 rpm, using distilled water, concentrated hydrochloric acid, and ethanol for removing the impurities. The obtained solid GO is vacuum dried at 55 °C for 11 h.

4.2. Synthesis of MTD-Chi/GO Bionanocomposite Beads. MTD-Chi/GO bionanocomposite beads were prepared by the gelation method. In short, chitosan (0.5 g) was stirred in 10 mL of distilled water. To this solution, different amounts of MTD drug (5−40 mg) were added (Table 2), followed by slow addition of oxalic acid (10.0 mg) as a chelating agent, and stirred for 2h to form an MTD-Chi mixture. Afterward, different quantities of GO (1.0−21.0 mg) were added to the MTD-Chi mixture (Table 2) and stirred for 2h to obtain a homogeneous solution of the MTD-Chi/GO bionanocomposite. Beads of the MTD-Chi/GO bionanocomposite were prepared through dropwise addition of the MTD-Chi/GO bionanocomposite using a 12.0 mL syringe with a 1 mm needle into NaOH (0.5 M) solution. The prepared beads were washed three times with distilled water. Scheme 1 shows the generalized steps involved in the preparation of MTD@Chi/GO bionanocomposite beads. The NaOH solution was used as a solvent for the preparation of the bionanocomposite beads. Moreover, a digital photograph of pure chitosan, MTD-Chi, and MTD-Chi/GO bionanocomposite beads is given in Figure S2.

Scheme 1. Illustration of the Steps Involved in the Preparation of the MTD-Chi/GO Bionanocomposite Beads

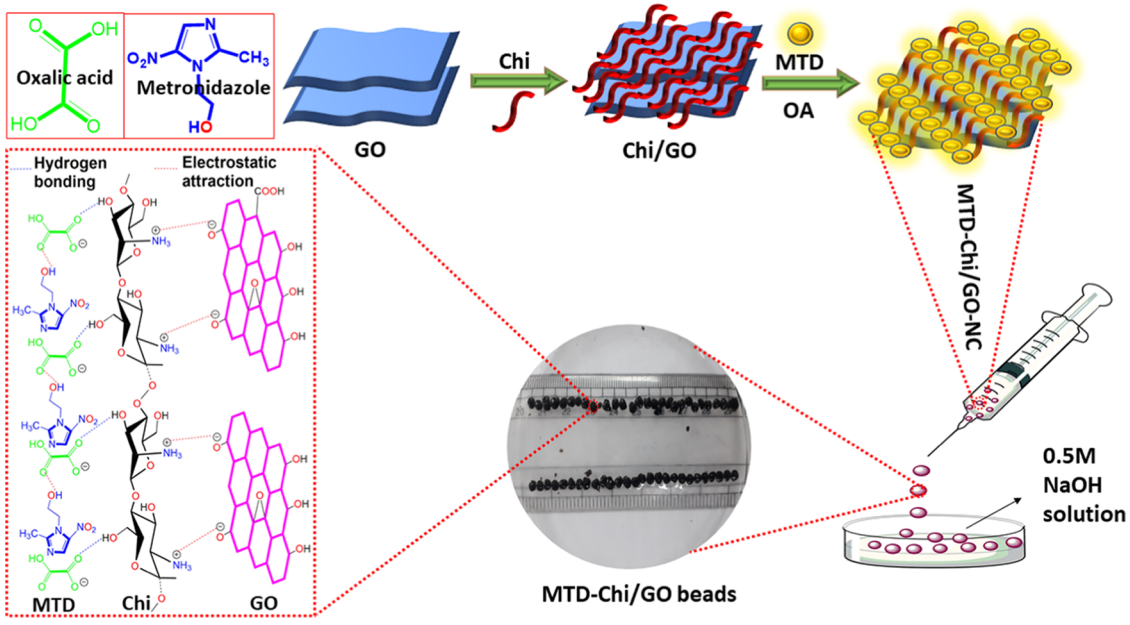

https://doi.org/10.1021/acsomega.1c02422
ACS Omega 2021, 6, 20433−20444

4.3. Swelling Ratio. The swelling ratio of the bionanocomposite beads was determined in accordance with previous literature.[80] The swelling ratio was calculated using the following eq 4.

$$\% \text{ swelling} = \left(\frac{w_1 - w_2}{w_2}\right) \times 1 \quad (4)$$

where w_1 is the weight of wet beads after 30 min of water immersion and w_2 is the initial weight of the dry beads.

5. MATERIALS AND METHODS

All chemicals applied to perform the experimental work were of analytical grade. Metronidazole and chitosan were obtained from Sigma-Aldrich. Terephthalic acid (H_2BDC) and natural graphite powder were purchased from SRL, India. Other chemicals such as hydrochloric acid, sodium hydroxide, potassium chloride, potassium dihydrogen phosphate, sodium acetate, and acetic acid were obtained from Merck. Double-distilled water was used throughout the experimental study.

The structural and morphological characterization of MTD-Chi/GO, Chi/GO, and GO was performed using various physicochemical techniques. Powder X-ray diffraction was performed using D8 Discover, Bruker, having Cu as the X-ray source between 2θ values of 5 and 80°. Fourier-transform infrared spectroscopy was performed using Spectrum RXI-Mid IR, PerkinElmer, in the range of 400−4000 cm^{-1}. Thermogravimetric analysis was done using PerkinElmer, Pyris diamond TGA/DTA in between 25 to 600 °C in the presence of air. Surface morphology and structural studies were performed using scanning electron microscopy (Model: JSM 6610LV, JEOL Japan) and transmission electron microscopy (TECNAI G20 HR-TEM, Thermo Scientific). Further X-ray photoelectron spectroscopy was performed using Model: PHI 5000 Versa Probe III, Physical Electronics. BET analysis was performed using ASI-CI-11, Quantachrome Instruments at an adsorbate temperature of 77 K. The supernatant MTD drug solutions were measured using a UV−visible spectrophotometer (UV 3092, LAB INDIA) instrument equipped with a quartz cell having a path length of 1 cm and data was recorded in the range of 200−400 nm. The analysis of the drug release pattern was done using the Dissolution Test Apparatus (DS 8000, LAB INDIA).

■ ASSOCIATED CONTENT

Supporting Information

The Supporting Information is available free of charge at https://pubs.acs.org/doi/10.1021/acsomega.1c02422.

Thermogravimetric analysis, digital photograph of MTD-Chi/GO bionanocomposite beads, and drug release kinetics (PDF)

■ AUTHOR INFORMATION

Corresponding Author

Dhanraj T. Masram − *Department of Chemistry, University of Delhi, Delhi 110007, India;* orcid.org/0000-0001-6273-8199; Email: Dhanraj_masram27@rediffmail.com

Authors

Gyanendra Kumar − *Department of Chemistry, University of Delhi, Delhi 110007, India;* orcid.org/0000-0002-1975-5310

Karan Chaudhary − *Department of Chemistry, University of Delhi, Delhi 110007, India*

Navin Kumar Mogha − *Shriram Institute for Industrial Research, Delhi 110007, India;* orcid.org/0000-0002-2483-1170

Arun Kant − *Department of Chemistry, University of Delhi, Delhi 110007, India*

Complete contact information is available at: https://pubs.acs.org/10.1021/acsomega.1c02422

Notes

The authors declare no competing financial interest.

■ ACKNOWLEDGMENTS

The authors are grateful to the Head, Department of Chemistry, University of Delhi, Delhi, India, and USIC for providing the necessary instrumentation facilities. The authors also acknowledge SAIF-AIIMS, New Delhi, for the TEM facilities. G.K. and K.C. are grateful to UGC for providing financial funding.

■ REFERENCES

(1) Dorati, R.; DeTrizio, A.; Modena, T.; Conti, B.; Benazzo, F.; Gastaldi, G.; Genta, I. Biodegradable Scaffolds for Bone Regeneration Combined with Drug-Delivery Systems in Osteomyelitis Therapy. *Pharmaceuticals* **2017**, *10*, No. 96.

(2) Kantor, M.; Abrantes, A.; Estevez, A.; Schiller, A.; Torrent, J.; Gascon, J.; Hernandez, R.; Ochner, C. Entamoeba Histolytica: Updates in Clinical Manifestation, Pathogenesis, and Vaccine Development. *Canadian J. Gastroenterol. Hepatol.* **2018**, *2018*, 1−6.

(3) Danao, K. R.; Hiradeve, S. M.; Moon, R. S.; Kasture, A. V.; Yeole, P. G. Simultaneous Estimation of Metronidazole and Diloxanide Furoate in Combination. *Int. J. Pharm. Life Sci.* **2010**, *1*, 82−85.

(4) Jia, H.; Kerr, L. L. Kinetics of Drug Release from Drug Carrier of Polymer/TiO2 Nanotubes Composite - PH Dependent Study *J. Appl. Polym. Sci.* 2015, *1327* DOI: 10.1002/app.41570.

(5) Elzatahry, A. A.; Eldin, M. S. M. Preparation and Characterization of Metronidazole-Loaded Chitosan Nanoparticles for Drug Delivery Application. *Polym. Adv. Technol.* **2008**, *19*, 1787−1791.

(6) Sabbagh, H. A. K.; Hussein-Al-Ali, S. H.; Hussein, M. Z.; Abudayeh, Z.; Ayoub, R.; Abudoleh, S. M. A Statistical Study on the Development of Metronidazole-Chitosan-Alginate Nanocomposite Formulation Using the Full Factorial Design. *Polymers* **2020**, *12*, No. 772.

(7) Ashford, M.; Fell, J. Targeting Drugs to the Colon: Delivery Systems for Oral Administration. *J. Drug Target.* **1994**, *2*, 241−257.

(8) Khalilzadeh, M. A.; Sadeghifar, H.; Venditti, R. Natural Clinoptilolite/Koh: An Efficient Heterogeneous Catalyst for Carboxymethylation of Hemicellulose. *Ind. Eng. Chem. Res.* **2019**, *58*, 11680−11688.

(9) Khalilzadeh, M. A.; Hosseini, S.; Rad, A. S.; Venditti, R. A. Synthesis of Grafted Nanofibrillated Cellulose-Based Hydrogel and Study of Its Thermodynamic, Kinetic, and Electronic Properties. *J. Agric. Food Chem.* **2020**, *68*, 8710−8719.

(10) Kalantari, E.; Khalilzadeh, M. A.; Zareyee, D. Effective Reduction of Cr(VI) and Organic Dyes Using Pd NPs/Fe3O4@ nanocellulose as a Recoverable Catalyst in Aqueous Media. *J. Inorg. Organomet. Polym. Mater.* **2021**, *31*, 319−330.

(11) Seyednejhad, S.; Khalilzadeh, M. A.; Zareyee, D.; Sadeghifar, H.; Venditti, R. Cellulose Nanocrystal Supported Palladium as a Novel Recyclable Catalyst for Ullmann Coupling Reactions. *Cellulose* **2019**, *26*, 5015−5031.

(12) Amirsoleimani, M.; Khalilzadeh, M. A.; Sadeghifar, F.; Sadeghifar, H. Surface Modification of Nanosatrch Using Nano

Silver: A Potential Antibacterial for Food Package Coating. *J. Food Sci. Technol.* **2018**, *55*, 899−904.
(13) Kalantari, E.; Khalilzadeh, M. A.; Zareyee, D.; Shokouhimehr, M. Catalytic Degradation of Organic Dyes Using Green Synthesized Fe3O4-Cellulose-Copper Nanocomposites. *J. Mol. Struct.* **2020**, *1218*, No. 128488.
(14) Alcântara, A. C. S.; Aranda, P.; Darder, M.; Ruiz-Hitzky, E. Bionanocomposites Based on Alginate-Zein/Layered Double Hydroxide Materials as Drug Delivery Systems. *J. Mater. Chem.* **2010**, *20*, 9495−9504.
(15) Wan Ngah, W. S.; Teong, L. C.; Hanafiah, M. A. K. M. Adsorption of Dyes and Heavy Metal Ions by Chitosan Composites: A Review. *Carbohydr. Polym.* **2011**, *1*, 1446−1456.
(16) Mohammadzadeh Pakdel, P.; Peighambardoust, S. J. Review on Recent Progress in Chitosan-Based Hydrogels for Wastewater Treatment Application. *Carbohydr. Polym.* **2018**, *1*, 264−279.
(17) Makhado, E.; Pandey, S.; Nomngongo, P. N.; Ramontja, J. Preparation and Characterization of Xanthan Gum-Cl-Poly(Acrylic Acid)/o-MWCNTs Hydrogel Nanocomposite as Highly Effective Re-Usable Adsorbent for Removal of Methylene Blue from Aqueous Solutions. *J. Colloid Interface Sci.* **2018**, *513*, 700−714.
(18) Makhado, E.; Pandey, S.; Nomngongo, P. N.; Ramontja, J. Fast Microwave-Assisted Green Synthesis of Xanthan Gum Grafted Acrylic Acid for Enhanced Methylene Blue Dye Removal from Aqueous Solution. *Carbohydr. Polym.* **2017**, *176*, 315−326.
(19) Dash, M.; Chiellini, F.; Ottenbrite, R. M.; Chiellini, E. Chitosan - A Versatile Semi-Synthetic Polymer in Biomedical Applications. *Prog. Polym. Sci.* **2011**, *1*, 981−1014.
(20) Prabaharan, M. Review Paper: Chitosan Derivatives as Promising Materials for Controlled Drug Delivery. *J. Biomater. Appl.* **2008**, *23*, 5−36.
(21) Elgadir, M. A.; Uddin, M. S.; Ferdosh, S.; Adam, A.; Chowdhury, A. J. K.; Sarker, M. Z. I. Impact of Chitosan Composites and Chitosan Nanoparticle Composites on Various Drug Delivery Systems: A Review. *J. Food Drug Anal.* **2015**, *1*, 619−629.
(22) Shtenberg, Y.; Goldfeder, M.; Prinz, H.; Shainsky, J.; Ghantous, Y.; Abu El-Naaj, I.; Schroeder, A.; Bianco-Peled, H. Mucoadhesive Alginate Pastes with Embedded Liposomes for Local Oral Drug Delivery. *Int. J. Biol. Macromol.* **2018**, *111*, 62−69.
(23) Hamidian, H.; Tavakoli, T. Preparation of a New Fe3O4/Starch-g-Polyester Nanocomposite Hydrogel and a Study on Swelling and Drug Delivery Properties. *Carbohydr. Polym.* **2016**, *144*, 140−148.
(24) Yadollahi, M.; Gholamali, I.; Namazi, H.; Aghazadeh, M. Synthesis and Characterization of Antibacterial Carboxymethylcellulose/CuO Bio-Nanocomposite Hydrogels. *Int. J. Biol. Macromol.* **2015**, *73*, 109−114.
(25) Archana, D.; Dutta, J.; Dutta, P. K. Evaluation of Chitosan Nano Dressing for Wound Healing: Characterization, in Vitro and in Vivo Studies. *Int. J. Biol. Macromol.* **2013**, *57*, 193−203.
(26) Martínez-Martínez, M.; Rodríguez-Berna, G.; Gonzalez-Alvarez, I.; Hernández, M.; Corma, A.; Bermejo, M.; Merino, V.; Gonzalez-Alvarez, M. Ionic Hydrogel Based on Chitosan Cross-Linked with 6-Phosphogluconic Trisodium Salt as a Drug Delivery System. *Biomacromolecules* **2018**, *19*, 1294−1304.
(27) Jayakumar, R.; Nwe, N.; Tokura, S.; Tamura, H. Sulfated Chitin and Chitosan as Novel Biomaterials. *Int. J. Biol. Macromol.* **2007**, *28*, 175−181.
(28) Xiao, B.; Chen, Q.; Zhang, Z.; Wang, L.; Kang, Y.; Denning, T.; Merlin, D. TNFα Gene Silencing Mediated by Orally Targeted Nanoparticles Combined with Interleukin-22 for Synergistic Combination Therapy of Ulcerative Colitis. *J. Controlled Release* **2018**, *287*, 235−246.
(29) Xie, M.; Lei, H.; Zhang, Y.; Xu, Y.; Shen, S.; Ge, Y.; Li, H.; Xie, J. Non-Covalent Modification of Graphene Oxide Nanocomposites with Chitosan/Dextran and Its Application in Drug Delivery. *RSC Adv.* **2016**, *6*, 9328−9337.
(30) Kyzas, G. Z.; Kostoglou, M.; Lazaridis, N. K.; Bikiaris, D. N. N-(2-Carboxybenzyl) Grafted Chitosan as Adsorptive Agent for Simultaneous Removal of Positively and Negatively Charged Toxic Metal Ions. *J. Hazard. Mater.* **2013**, *244*−*245*, 29−38.
(31) Debnath, S.; Parashar, K.; Pillay, K. Ultrasound Assisted Adsorptive Removal of Hazardous Dye Safranin O from Aqueous Solution Using Crosslinked Graphene Oxide-Chitosan (GO[Sbnd]-CH) Composite and Optimization by Response Surface Methodology (RSM) Approach. *Carbohydr. Polym.* **2017**, *175*, 509−517.
(32) Lewandowska, K.; Sionkowska, A.; Kaczmarek, B.; Furtos, G. Characterization of Chitosan Composites with Various Clays. *Int. J. Biol. Macromol.* **2014**, *65*, 534−541.
(33) Peng, Q.; Liu, M.; Zheng, J.; Zhou, C. Adsorption of Dyes in Aqueous Solutions by Chitosan-Halloysite Nanotubes Composite Hydrogel Beads. *Microporous Mesoporous Mater.* **2015**, *201*, 190−201.
(34) Zhao, X.; Guo, B.; Wu, H.; Liang, Y.; Ma, P. X. Injectable Antibacterial Conductive Nanocomposite Cryogels with Rapid Shape Recovery for Noncompressible Hemorrhage and Wound Healing. *Nat. Commun.* **2018**, *9*, No. 2784.
(35) Zhang, Y.; Guan, J.; Wu, J.; Ding, S.; Yang, J.; Zhang, J.; Dong, A.; Deng, L. N-Alkylated Chitosan/Graphene Oxide Porous Sponge for Rapid and Effective Hemostasis in Emergency Situations. *Carbohydr. Polym.* **2019**, *219*, 405−413.
(36) Subodh; Mogha, N. K.; Chaudhary, K.; Kumar, G.; Masram, D. T. Fur-Imine-Functionalized Graphene Oxide-Immobilized Copper Oxide Nanoparticle Catalyst for the Synthesis of Xanthene Derivatives. *ACS Omega* **2018**, *3*, 16377−16385.
(37) Liu, Z.; Robinson, J. T.; Sun, X.; Dai, H. PEGylated Nanographene Oxide for Delivery of Water-Insoluble Cancer Drugs. *J. Am. Chem. Soc.* **2008**, *130*, 10876−10877.
(38) Mianehrow, H.; Afshari, R.; Mazinani, S.; Sharif, F.; Abdouss, M. Introducing a Highly Dispersed Reduced Graphene Oxide Nano-Biohybrid Employing Chitosan/Hydroxyethyl Cellulose for Controlled Drug Delivery. *Int. J. Pharm.* **2016**, *509*, 400−407.
(39) Wang, C.; Chen, B.; Zou, M.; Cheng, G. Cyclic RGD-Modified Chitosan/Graphene Oxide Polymers for Drug Delivery and Cellular Imaging. *Colloids Surf., B* **2014**, *122*, 332−340.
(40) Goenka, S.; Sant, V.; Sant, S. Graphene-Based Nanomaterials for Drug Delivery and Tissue Engineering. *J. Controlled Release* **2014**, *10*, 75−88.
(41) Al-Omar, M. A.; Al-Mohizea, A. M. Famotidine. In *Profiles of Drug Substances, Excipients and Related Methodology*; Academic Press Inc: 2008; *Vol. 34*, Chapter 3, 115−151.
(42) Kumar, G.; Masram, D. T. Sustainable Synthesis of MOF-5@GO Nanocomposites for Efficient Removal of Rhodamine B from Water. *ACS Omega* **2021**, *6*, 9587−9599.
(43) Liu, J.; Dong, J.; Zhang, T.; Peng, Q. Graphene-Based Nanomaterials and Their Potentials in Advanced Drug Delivery and Cancer Therapy. *J. Controlled Release* **2018**, *28*, 64−73.
(44) Kumar, G.; Mogha, N. K.; Masram, D. T. Zr-Based Metal−Organic Framework/Reduced Graphene Oxide Composites for Catalytic Synthesis of 2,3-Dihydroquinazolin-4(1 *H*)-One Derivatives. *ACS Appl. Nano Mater.* **2021**, *4*, 2682−2693.
(45) Liu, Z.; Tabakman, S.; Welsher, K.; Dai, H. Carbon Nanotubes in Biology and Medicine: In Vitro and in Vivo Detection, Imaging and Drug Delivery. *Nano Res.* **2009**, *2*, 85−120.
(46) Yang, Y.; Asiri, A. M.; Tang, Z.; Du, D.; Lin, Y. Graphene Based Materials for Biomedical Applications. *Materials Today.* **2013**, *16*, 365−373.
(47) Bao, H.; Pan, Y.; Ping, Y.; Sahoo, N. G.; Wu, T.; Li, L.; Li, J.; Gan, L. H. Chitosan-Functionalized Graphene Oxide as a Nanocarrier for Drug and Gene Delivery. *Small* **2011**, *7*, 1569−1578.
(48) Sun, X.; Liu, Z.; Welsher, K.; Robinson, J. T.; Goodwin, A.; Zaric, S.; Dai, H. Nano-Graphene Oxide for Cellular Imaging and Drug Delivery. *Nano Res.* **2008**, *1*, 203−212.
(49) Sivashankari, P. R.; Prabaharan, M. Chitosan/Carbon-Based Nanomaterials as Scaffolds for Tissue Engineering. In *Biopolymer-Based Composites: Drug Delivery and Biomedical Applications*; Elsevier, 2017; pp 381−397.
(50) Peng, H.; Huang, Z.; Zheng, Y.; Chen, W.; Liu, A.; Lin, X. A Novel Nanocomposite Matrix Based on Graphene Oxide and

https://doi.org/10.1021/acsomega.1c02422
ACS Omega 2021, 6, 20433−20444

Ferrocene-Branched Organically Modified Sol-Gel/Chitosan for Biosensor Application. *J. Solid State Electrochem.* **2014**, *18*, 1941−1949.
(51) Yu, P.; Bao, R. Y.; Shi, X. J.; Yang, W.; Yang, M. B. Self-Assembled High-Strength Hydroxyapatite/Graphene Oxide/Chitosan Composite Hydrogel for Bone Tissue Engineering. *Carbohydr. Polym.* **2017**, *155*, 507−515.
(52) Lin, K.-F.; Hsu, C.-Y.; Huang, T.-S.; Chiu, W.-Y.; Lee, Y.-H.; Young, T.-H. A Novel Method to Prepare Chitosan/Montmorillonite Nanocomposites. *J. Appl. Polym. Sci.* **2005**, *98*, 2042−2047.
(53) Moussout, H.; Ahlafi, H.; Aazza, M.; Amechrouq, A. Bentonite/Chitosan Nanocomposite: Preparation, Characterization and Kinetic Study of Its Thermal Degradation. *Thermochim. Acta* **2018**, *659*, 191−202.
(54) Al-Gaashani, R.; Najjar, A.; Zakaria, Y.; Mansour, S.; Atieh, M. A. XPS and Structural Studies of High Quality Graphene Oxide and Reduced Graphene Oxide Prepared by Different Chemical Oxidation Methods. *Ceram. Int.* **2019**, *45*, 14439−14448.
(55) Mahanta, A. K.; Senapati, S.; Maiti, P. A Polyurethane-Chitosan Brush as an Injectable Hydrogel for Controlled Drug Delivery and Tissue Engineering. *Polym. Chem.* **2017**, *8*, 6233−6249.
(56) Kosowska, K.; Domalik-Pyzik, P.; Nocuń, M.; Chłopek, J. Chitosan and Graphene Oxide/Reduced Graphene Oxide Hybrid Nanocomposites − Evaluation of Physicochemical Properties. *Mater. Chem. Phys.* **2018**, *216*, 28−36.
(57) Mogha, N. K.; Kirti, S.; Masram, D. T. La_2O_3/Reduced Graphene Oxide Nanocomposite: A Highly Efficient, Reusable Heterogeneous Catalyst for the Synthesis of Biologically Important Bis(Indolyl)Methanes under Solvent Free Conditions. *J. Nanosci. Nanotechnol.* **2017**, *17*, 2508−2514.
(58) Chaudhary, K.; Kumar, K.; Venkatesu, P.; Masram, D. T. In-Depth Understanding of a Nano-Bio Interface between Lysozyme and Au NP-Immobilized N-Doped Reduced Graphene Oxide 2-D Scaffolds. *Nanoscale Adv.* **2020**, *2*, 2146−2159.
(59) Shavandi, A.; Bekhit, A. A.; Bekhit, A. E. D. A.; Sun, Z.; Ali, M. A. Preparation and Characterisation of Irradiated Crab Chitosan and New Zealand Arrow Squid Pen Chitosan. *Mater. Chem. Phys.* **2015**, *167*, 295−302.
(60) Kumar, G.; Kant, A.; Kumar, M.; Masram, D. T. Synthesis, Characterizations and Kinetic Study of Metal Organic Framework Nanocomposite Excipient Used as Extended Release Delivery Vehicle for an Antibiotic Drug. *Inorganica Chim. Acta* **2019**, *496*, No. 119036.
(61) Parhizkar, N.; Shahrabi, T.; Ramezanzadeh, B. A New Approach for Enhancement of the Corrosion Protection Properties and Interfacial Adhesion Bonds between the Epoxy Coating and Steel Substrate through Surface Treatment by Covalently Modified Amino Functionalized Graphene Oxide Film. *Corros. Sci.* **2017**, *123*, 55−75.
(62) Cheng, F.; Sajedin, S. M.; Kelly, S. M.; Lee, A. F.; Kornherr, A. UV-Stable Paper Coated with APTES-Modified P25 TiO2 Nanoparticles. *Carbohydr. Polym.* **2014**, *114*, 246−252.
(63) Kehrer, M.; Duchoslav, J.; Hinterreiter, A.; Cobet, M.; Mehic, A.; Stehrer, T.; Stifter, D. XPS Investigation on the Reactivity of Surface Imine Groups with TFAA. *Plasma Process. Polym.* **2019**, *16*, No. 1800160.
(64) Schmiers, H.; Friebel, J.; Streubel, P.; Hesse, R.; Köpsel, R. Change of Chemical Bonding of Nitrogen of Polymeric N-Heterocyclic Compounds during Pyrolysis. *Carbon* **1999**, *37*, 1965−1978.
(65) Mekki, A.; Holland, D.; Ziq, K. A.; McConville, C. F. Structural and Magnetic Properties of Sodium Iron Germanate Glasses. *J. Non. Cryst. Solids* **2000**, *272*, 179−190.
(66) Yadav, M.; Rhee, K. Y.; Park, S. J.; Hui, D. Mechanical Properties of Fe_3O_4/GO/Chitosan Composites. *Composites, Part B* **2014**, *66*, 89−96.
(67) Zuo, P.-P.; Feng, H. F.; Xu, Z. Z.; Zhang, L. F.; Zhang, Y. L.; Xia, W.; Zhang, W. Q. Fabrication of Biocompatible and Mechanically Reinforced Graphene Oxide-Chitosan Nanocomposite Films. *Chem. Cent. J.* **2013**, *7*, No. 39.
(68) Jia, J.; Gai, Y.; Wang, W.; Zhao, Y. Green Synthesis of Biocompatiable Chitosan-Graphene Oxide Hybrid Nanosheet by Ultrasonication Method. *Ultrason. Sonochem.* **2016**, *32*, 300−306.
(69) Kim, M.; Hong, J.; Lee, J.; Hong, C. K.; Shim, S. E. Fabrication of Silica Nanotubes Using Silica Coated Multi-Walled Carbon Nanotubes as the Template. *J. Colloid Interface Sci.* **2008**, *322*, 321−326.
(70) Fang, Q.; Chen, B. Self-Assembly of Graphene Oxide Aerogels by Layered Double Hydroxides Cross-Linking and Their Application in Water Purification. *J. Mater. Chem. A* **2014**, *2*, 8941−8951.
(71) Dash, S.; Murthy, P. N.; Nath, L.; Chowdhury, P. Kinetic Modeling on Drug Release from Controlled Drug Delivery Systems. *Acta Pol. Pharm. - Drug Res.* **2010**, 217−223.
(72) Chen, W.; Yan, L.; Bangal, P. R. Chemical Reduction of Graphene Oxide to Graphene by Sulfur-Containing Compounds. *J. Phys. Chem. C* **2010**, *114*, 19885−19890.
(73) Ritger, P. L.; Peppas, N. A. A Simple Equation for Description of Solute Release II. Fickian and Anomalous Release from Swellable Devices. *J. Controlled Release* **1987**, *5*, 37−42.
(74) Li, Y.; Jiang, L. Preparation of Graphene Oxide-Chitosan Nanocapsules and Their Applications as Carriers for Drug Delivery. *RSC Adv.* **2016**, *6*, 104522−104528.
(75) Mahajan, C. R.; Joshi, L. B.; Varma, U.; Naik, J. B.; Chaudhari, V. R.; Mishra, S. Sustainable Drug Delivery of Famotidine Using Chitosan-Functionalized Graphene Oxide as Nanocarrier. *Glob. Challenges* **2019**, *3*, No. 1900002.
(76) Jafari, Z.; Rad, A. S.; Baharfar, R.; Asghari, S.; Esfahani, M. R. Synthesis and Application of Chitosan/Tripolyphosphate/Graphene Oxide Hydrogel as a New Drug Delivery System for Sumatriptan Succinate. *J. Mol. Liq.* **2020**, *315*, No. 113835.
(77) Hosseini, S. M.; Mazinani, S.; Abdouss, M.; Kalhor, H.; Kalantari, K.; Amiri, I. S.; Ramezani, Z. Designing Chitosan Nanoparticles Embedded into Graphene Oxide as a Drug Delivery System. *Polym. Bull.* **2021**, 1−14.
(78) Kumar, G.; Mogha, N. K.; Kumar, M.; Subodh; Masram, D. T. NiO Nanocomposites/RGO as a Heterogeneous Catalyst for Imidazole Scaffolds with Applications in Inhibiting the DNA Binding Activity. *Dalt. Trans.* **2020**, *49*, 1963−1974.
(79) Marcano, D. C.; Kosynkin, D. V.; Berlin, J. M.; Sinitskii, A.; Sun, Z.; Slesarev, A.; Alemany, L. B.; Lu, W.; Tour, J. M. Improved Synthesis of Graphene Oxide. *ACS Nano* **2010**, *4*, 4806−4814.
(80) Timur, M.; Paşa, A. Synthesis, Characterization, Swelling, and Metal Uptake Studies of Aryl Cross-Linked Chitosan Hydrogels. *ACS Omega* **2018**, *3*, 17416−17424.

https://doi.org/10.1021/acsomega.1c02422
ACS Omega 2021, 6, 20433−20444